

**OPTIMUM LAUNCH TRAJECTORIES FOR THE ATS-E MISSION**

by Omer F. Spurlock and Fred Teren

Lewis Research Center  
Cleveland, Ohio

TECHNICAL PAPER proposed for presentation at  
Astrodynamics Conference  
sponsored by the American Astronautical Society and the  
American Institute of Aeronautics and Astronautics  
Santa Barbara, California, August 20-21, 1970

**NATIONAL AERONAUTICS AND SPACE ADMINISTRATION**

# OPTIMUM LAUNCH TRAJECTORIES FOR THE ATS-E MISSION

by Omer F. Spurlock and Fred Teren

Lewis Research Center  
National Aeronautics and Space Administration  
Cleveland, Ohio

## Abstract

Optimum trajectories for the Applications Technology Satellite (ATS)-E mission are obtained. Analysis, procedure, and results are presented. The trajectories are numerically integrated from launch to insertion into the final orbit. As a result of a much smaller than optimum apogee motor, these trajectories, unlike conventional synchronous orbit trajectories, require non-circular parking orbits and large amounts of inclination reduction before the solid motor burn at apogee. Constraints on parking orbit perigee radius and duration are included. Figures are presented describing the results.

## Introduction

The Applications Technology Satellite (ATS)-E mission is a circular synchronous equatorial orbit mission. The ATS program has the objective of advancing technology in areas which may have application to future spacecraft. The experiments which are conducted are spacecraft, communication, and science oriented.

The spacecraft-oriented experiments on the ATS-E provide information on power supply and control systems, a gravity-gradient stabilization system, resistojet and ion micropound thrusters, and synchronous environment. The scientific-oriented experiments gather data on the particle (electron and proton) distribution and flux and the character of the electric and magnetic fields at synchronous altitude.

The launch vehicle for the ATS-E mission was an Atlas-Centaur and the solid apogee motor was a part of the spacecraft system. The apogee motor total impulse was sized for the early ATS missions on the Atlas-Agena launch vehicle, which has less payload capability than the Atlas-Centaur. The apogee motor, although smaller than optimum for the larger vehicle, remained unchanged.

For an optimally sized apogee motor, a conventional trajectory to circular synchronous equatorial orbit is near optimum. A conventional trajectory consists of five consecutive phases as shown in Fig. 1. The first phase is an ascent from the launch site to a circular parking orbit. To maximize the mass in orbit, a  $90^\circ$  launch azimuth is used, which results in a parking orbit inclination equal to the launch site latitude. This inclination must be removed during the trajectory. The second phase is a coast arc to the proximity of the equator. A small portion of the required plane change is removed by the second burn, the third phase. Much more importantly, the second burn must place the vehicle in a transfer orbit whose apogee is over the equator and equal to synchronous altitude. The vehicle coasts to apogee in the fourth phase. The fifth phase consists of a final burn that removes the major portion of the inclination and circularizes the orbit.

Intuitively, it seems reasonable that this conventional profile is near optimum if the burn and coast durations may be varied to maximize the mass at the end of each burn. However, if the total impulse of the final burn is fixed at less than the optimum value, the conventional trajectory must be modified to yield maximum payload to the final orbit. In particular, the parking orbit is noncircular, the perigee radius of the transfer orbit increases, and the second burn removes more than a minor part of the inclination. The optimization problem is to find the best combination of these changes and other less important ones to yield maximum payload to circular synchronous equatorial orbit.

Optimization of the conventional trajectory to circular synchronous equatorial orbit has been treated by several authors. Hoelker and Silber<sup>(1)</sup> present a detailed analysis of the conventional problem. Rider<sup>(2)</sup> considers the problem of changing the plane and also the radius of a circular orbit. These and other similar studies treat the problem as one of changing the plane and radius of a circular orbit, ignoring the ascent to the first (parking) circular orbit. This is satisfactory for the conventional case. However, an unconventional trajectory is more complex since the parking orbit is in general noncircular. The ascent must be included as part of the optimization problem. Therefore, a more sophisticated optimization procedure is required for unconventional trajectories. Additionally, the references mentioned above are general and consequently are not concerned with constraints which may alter the acceptability of a given trajectory, such as limitations on coast time or the minimum perigee radius of the noncircular parking orbit.

The problem of optimizing trajectories to circular synchronous equatorial orbit may be considered as a multistage launch vehicle optimization. Several analyses have been performed to optimize multistage launch vehicles, including one by the authors of this report<sup>(3)</sup>. For optimizing the unconventional trajectory, the analysis in Ref. 3 was expanded to three dimensions and also, to include a constraint on the parking orbit perigee radius. The perigee radius constraint must be included to limit aerodynamic heating on the spacecraft.

The Applications Technology Satellite (ATS)-E mission on the Atlas-Centaur vehicle requires an unconventional trajectory to achieve maximum payload. The final burn is performed by a solid motor which is part of the spacecraft system. That motor is significantly smaller than optimum. There are spacecraft and launch vehicle constraints on the trajectory which must be incorporated into the solution. The perigee radius and the parking orbit coast duration are limited. The results for this mission are presented.

Problem Description

A conventional trajectory to circular synchronous equatorial orbit launched from the Eastern Test Range consists of five phases. They are:

1. Ascent to parking orbit.
2. Parking orbit coast.
3. Second impulse.
4. Transfer orbit coast.
5. Third impulse or apogee burn.

Figure 1 shows the planar characteristics of the conventional trajectory. The nonplanar characteristics are shown in Fig. 2. The vehicle is launched at an azimuth of  $90^\circ$  in order to maximize the vehicle mass in parking orbit and to minimize the inclination of the parking orbit. The circular parking orbit altitude is as low as aerodynamic heating constraints will allow, usually about 165 to 185 kilometers. The parking orbit coast time is usually about fifteen minutes - the time required to coast from orbit insertion to the first equator crossing. The third phase places the vehicle in a transfer orbit whose apogee and perigee are over the equator. The apogee altitude is about equal to the required altitude for a circular synchronous orbit. The transfer orbit coast time is about five and one-half hours. The third impulse, the apogee burn, occurs at apogee of the transfer orbit. Apogee is designed to occur at the equator and at the proper altitude for injection into the final orbit. A small part of the inclination is removed by the second impulse with the remainder being removed by the apogee burn. In this conventional method, the final conditions at the end of each burn are known and the mass can easily be maximized progressively phase by phase if the second and third impulse sizes are unspecified.

Now suppose that the total impulse of the third burn is fixed. Then the transfer orbit must be constructed such that the  $\Delta V$  available from the third impulse is exactly that required to place the vehicle in circular synchronous equatorial orbit. If the  $\Delta V$  available from a fixed third total impulse is less than that required to circularize and equatorialize the orbit for the mass available from a conventional ascent and second impulse, then the trajectory to transfer orbit insertion must be altered to reduce the  $\Delta V$  required of the third impulse. This can be done by reducing the required plane change and the  $\Delta V$  required for circularization. For reasons described at length in the Results and Discussion section, the unconventional trajectory needed to reduce the  $\Delta V$  required of the apogee motor varies in many respects from the conventional profile. The most dramatic changes are a noncircular parking orbit, nontrivial inclination reduction by the second impulse, and a significantly nonequatorial latitude for the second impulse. As is desired, the changes result in lowering the  $\Delta V$  required of the fixed apogee motor. However, in this unconventional profile, the final conditions required at the end of the ascent and second impulse are unknown. They might be determined by varying those final conditions parametrically until the optimum is obtained. However, because of the number of variables, this process is clumsy and time consuming.

A Calculus of Variations formulation was used to maximize the payload to circular synchronous equatorial orbit without resorting to a parametric search. The optimization of the atmospheric portion of the trajectory is omitted from the variational analysis since the steering is constrained by factors other than optimizing performance, such as aerodynamic loading and heating limitations. The analysis considers the problem from the point in the trajectory that the atmosphere can be neglected to insertion into the final orbit. In addition to optimizing the steering, the durations of any unspecified burns and coasts are optimized while maintaining the specified perigee radius of the parking orbit. The analysis is presented in appendix B. It is derived in three dimensional rectangular coordinates in a manner similar to Ref. 4. The equations for optimum burn and coast duration are obtained from an analysis similar to that used by the authors in Ref. 3. It is necessary to extend the analysis to include an intermediate boundary condition which specifies the perigee radius of the parking orbit at the end of the ascent. Additionally, the oblate earth model must be added to the variational analysis. The effect of oblateness is not negligible in trajectories to circular synchronous equatorial orbit. Trajectories to that orbit are long, minimally around six hours. Oblateness is the major perturbing force during most of a trajectory. Because of the large change in inclination required to perform the mission, any perturbation in the inclination, thus increasing or decreasing the amount of plane change required of the propulsion systems, affects the final mass and should be considered in the analysis.

The trajectories are numerically integrated to incorporate a nonimpulsive vehicle model and to include the effects of oblateness and small thrusts over long periods of time which cannot be conveniently treated impulsively.

The analysis presented in appendix B requires the solution of a two point boundary value problem. The solution to the two point boundary value problem for the circular synchronous orbit problem with a fixed apogee burn and parking orbit coast time requires satisfaction of a minimum of eight final conditions with an equal number of initial conditions. The number and specific initial and final conditions are explained in appendix B.

Procedure

A simple Newton Raphson iteration scheme was used to solve the two point boundary value problem. This scheme was used successfully with as many as twelve iteration variables. For further explanation of the iteration scheme, see Ref. 5.

The partial derivatives required for the iteration scheme were obtained by integrating the adjoint equations. These were obtained as in Ref. 4. Solutions were initially obtained by using a spherical earth model for the adjoint equations, but it was found that including the oblateness terms improved the convergence properties of the problems. In some problems of this type, it was found that including the oblateness terms was necessary to obtain convergence.

It was difficult to obtain solutions to these problems because of the high degree of nonlinearity of many of the derivatives as well as the difficulty of guessing at the initial values of the thrust angle in pitch and yaw and their rates. A technique was devised to systematically proceed from a simple, easily converged problem to the final solution. This technique is described at length in appendix C. Other techniques, such as gradient methods, might avoid some of the difficulties associated with the Newton Raphson technique. However, the method described in the appendix is convenient, straightforward, and adequate. After obtaining one solution, proceeding to others in the region of interest is not difficult.

## Results and Discussion

### I. Launch Vehicle

The spacecraft is launched by an Atlas-Centaur, a two-and-a-half stage vehicle. The Atlas is propelled by two booster engines and one sustainer engine. The booster engines are jettisoned at a predetermined acceleration level. The sustainer engine continues to burn (sustainer solo). The Centaur insulation panels and then the payload fairing are jettisoned in this phase. The sustainer solo ends at propellant depletion and the Atlas stage is jettisoned. After about ten seconds, the Centaur engines, burning hydrogen and oxygen, ignite and burn until the desired parking orbit is reached. During the parking orbit, a hydrogen peroxide propulsion system is used to maintain a very small acceleration for propellant retention and for attitude control. At the end of the parking orbit, the Centaur engines burn again until the proper transfer orbit is achieved. After engine shutdown, the Centaur control system acquires the proper orientation for the spacecraft burn, the Centaur and the spacecraft separate, and the spacecraft is spun up for stability. The spacecraft coasts up to the proper altitude maintaining the separation attitude. The spacecraft motor burns to place the spacecraft in the final orbit. The spacecraft apogee motor has thrust of 22 240 newtons and an effective specific impulse of 279.1 seconds. The total impulse available from the motor is 950 900 newton-seconds, which corresponds to a propellant load of 347 kilograms.

### II. Trajectory Description

The trajectory starts with a short vertical rise, followed by a rapid pitchover phase in the desired azimuth direction. The amount of pitchover determines the amount of lofting during the atmospheric portion of the trajectory. The remainder of the atmospheric phase (which is assumed to end at booster stage jettison), is flown with a near-zero angle of attack steering program (described in Ref. 5), to minimize vehicle heating and aerodynamic loads. The thrust direction is constrained to be parallel to the launch azimuth plane, which is established at launch.

Since the ATS-E spacecraft motor has a fixed propellant load, the trajectory must be designed such that the  $\Delta V$  required at apogee of the transfer orbit is exactly that required to place the spacecraft in the desired final orbit. As mentioned earlier, the ATS-E motor is much smaller than optimum. The Atlas-Centaur can put more mass in a con-

ventional transfer orbit than the apogee motor can place in circular synchronous equatorial orbit. Therefore, an unconventional trajectory is required to lower the  $\Delta V$  required of the apogee burn.

An optimum unconventional trajectory was obtained for the ATS-E mission to circular synchronous equatorial orbit. The  $\Delta V$  required of the apogee motor is reduced by decreasing each of the two components which together make up the total  $\Delta V$  - that needed to circularize the orbit and to reduce the inclination to zero. The  $\Delta V$  for circularization is reduced by increasing the horizontal velocity at apogee of the transfer orbit without adding radial velocity. Any radial velocity would have to be removed by the apogee burn. Increasing the horizontal velocity at a fixed apogee radius is equivalent to raising the perigee radius of the transfer orbit - thereby decreasing the ellipticity of the transfer orbit.

The  $\Delta V$  required at apogee for reducing the inclination to zero is decreased by lowering the inclination of the transfer orbit. However, raising the velocity at apogee increases the  $\Delta V$  required for inclination removal at a fixed transfer orbit inclination. Therefore, the combination of the two methods represents a compromise which is optimized as part of the total problem.

In order to obtain the modified transfer orbit, the trajectory to insertion into that orbit is modified. Most of the inclination reduction is performed by the second burn near the equator. Only a small part of the inclination change to transfer orbit insertion is accomplished in the ascent to parking orbit.

The characteristics of the optimum parking orbit are changed from the conventional profile to increase the perigee radius of the transfer orbit. An elliptical rather than circular parking orbit is used to raise the altitude of the second burn. The perigee radius of the optimum parking orbit remains limited by aerodynamic heating consideration at some acceptable value. Since injection into the parking orbit occurs near perigee, the vehicle must coast along the ellipse to a higher radius. Due to limitation of the coast duration for the ATS-E mission, the second burn was required to occur near the first equator crossing. (From tracking or other considerations, a second (or greater) equator crossing could be chosen for the second burn, which would increase the parking orbit coast time by a half period (or more)). The latitude of the second burn is no longer equatorial as in the conventional case since the optimum position for raising the perigee radius and decreasing the inclination is dependent on radius and velocity as well as latitude. The parking orbit coast time is greater for this unconventional profile since the time to the equator is greater for an elliptical than for a circular parking orbit and additionally, the second burn occurs significantly south of the equator. Optimum true anomalies are found for the beginning and end of the parking and transfer orbit coasts. In addition, the optimum combination of the changes just described as characterizing the unconventional profile is selected.

The desired final inclination for the ATS-E mission is not exactly zero. The perturbations of the sun, moon, and oblateness of the earth cause

a spacecraft to drift from an exactly equatorial orbit. Since zero inclination is not a stable condition, a final orbit inclination yielding the smallest average inclination over the lifetime of the spacecraft is desired. Small final inclinations with the proper inertial ascending node are found to yield acceptable inclination over the lifetime of the satellite. The particular combinations of final orbit inclination and ascending node are functions of the positions of the sun and moon, which are in turn functions of launch time and date. Therefore, data were obtained for payload to circular synchronous orbits as a function of final inclination. Negative inclinations are included in the data. This convention indicates that the node has been switched approximately  $180^\circ$  by the apogee burn.

The Atlas-Centaur has a twenty-five minute limitation on parking orbit coast time for the mission. Therefore, inclusion of that constraint is necessary for realistic determination of vehicle capability. However, optimizing the coast time provides a more dramatic and obvious demonstration of the optimization procedure. Launch azimuth was not optimized along with the other trajectory parameters. The effect of launch azimuth was investigated parametrically to determine its effect on separated spacecraft mass.

Figure 3 presents separated spacecraft mass as a function of launch azimuth for final inclinations of  $(-2^\circ$  and  $5.25^\circ$  for both optimum and twenty-five minute parking orbit coast times. Separated spacecraft mass is the mass of the spacecraft when it is separated from the Centaur vehicle. This figure shows that the separated spacecraft mass is rather insensitive to launch azimuth. Hence, for simplicity, launch azimuth is fixed at  $90^\circ$  for the remaining figures.

Figure 4 shows the separated spacecraft mass as a function of final inclination. The separated spacecraft mass decreases as final inclination decreases. Figures 5 and 6 show the effect of final inclination on the transfer orbit inclination and inertial velocity at apogee. As might be expected, as the final inclination decreases, so does the transfer orbit inclination.

As might not be expected, the velocity at apogee also decreases as final inclination decreases. Figures 7 through 12 show why this occurs. Figure 7 shows the latitude of the second Centaur engine start as a function of final inclination. Since the second burn is required to remove more inclination as final inclination decreases, it is advantageous to move the burn nearer the equator for more efficient plane change. Figure 8 shows that the longitude of second burn start also decreases as final inclination decreases. These trends decrease the parking orbit coast arc as final inclination decreases. This is reflected in a decrease in the true anomaly at second Centaur cut-off, as seen in Fig. 9. Figures 10, 11, and 12 also show additional effects of moving the second burn nearer the equator. It decreases the parking orbit coast time, the altitude of the second burn, and the apogee altitude of the parking orbit. These all occur as a result of the decrease in parking orbit coast arc. These figures show why the apogee velocity is decreasing as final inclination decreases. The perigee

radius of the transfer orbit decreases as the altitude of the second burn decreases. The apogee altitude of the transfer orbit is almost constant at synchronous altitude, hence as perigee decreases, so does apogee velocity.

Figures 5 and 6 also indicate that more  $\Delta V$  is required of the apogee motor as final inclination decreases. It can be seen that both the plane change and circularization  $\Delta V$  are increasing. However, Fig. 4 shows that the ignition mass of the fixed solid motor is decreasing, which increases the  $\Delta V$  capability of the apogee motor.

Figure 13 shows the percentage of the Centaur propellant used in the first burn. The figure shows that as the final inclination increases, the first burn duration increases as the apogee altitude increases (Fig. 12).

The final longitude as a function of final inclination is shown in Fig. 14. It shows that longitude decreases as final inclination increases. The satellite remains at the longitude indicated only when the inclination is zero, the orbit circular, and the altitude synchronous. For other inclinations, the position (latitude and longitude) of the satellite subpoint describes a figure eight on the surface of the rotating earth. The longitudes indicated in Fig. 14 are injection longitudes, not necessarily the longitude at which the equator crossing occurs. For small inclinations, the longitude does not vary greatly during the period of the orbit.

Now consider the limitation of parking orbit coast time. Twenty-five minutes is less than optimum for all the final inclinations considered, as seen in Fig. 10. The differences in separated spacecraft mass are shown in Fig. 4. As seen from these figures, as the difference between the optimum and limited coast times decreases, the loss in payload due to coast time limitation decreases also.

The coast time limitation reduces the advantage of raising the apogee of the parking orbit as final inclination increases. The energy required to raise apogee does not yield the payload increases available with optimum coast time since the altitude cannot be acquired as efficiently in the shorter coast time. The energy is better spent by the second burn to reduce the inclination of the transfer orbit. This is reflected in several of the figures. In Fig. 5, the transfer orbit inclination for the coast limited case lies well below the optimum case. The lower second burn altitude is reflected in the lower velocity at apogee of the transfer orbit, as seen in Fig. 6. Because the parking orbit characteristics do not vary greatly with final inclination, the latitude and longitude of the second burn and the true anomaly at second Centaur cut-off are nearly constant. These may be seen in Figs. 7, 8, and 9. The conclusions which may be drawn for the percentage of Centaur propellant used in the first burn and final longitude (Figs. 13 and 14), are similar to those for the optimum coast case.

#### Summary of Conclusions

Analysis and results are presented for trajectories to circular synchronous equatorial orbit where the apogee motor is fixed at a smaller than

optimum total impulse. The results for the small apogee motor case were obtained for the ATS-E mission, which used the Atlas-Centaur launch vehicle.

The results show some of the characteristics of optimum trajectories for launch vehicle-apogee motor combinations where the apogee motor is smaller than optimum. More important, the results demonstrate that optimum trajectories to circular synchronous equatorial orbits may be obtained with detailed and hence complicated vehicle models for unconventional (small apogee motor) trajectory profiles. These results may be obtained without resorting to exotic mathematical procedures for solving the two point boundary value problem. These results were obtained with a simple Newton-Raphson iteration scheme. The partial derivatives were obtained by integrating the adjoint equations. The simple iteration scheme with the integrated partial derivatives is able to obtain solutions to the highly nonlinear two point boundary value problem even when the number of initial and final conditions reaches twelve.

#### Appendix A

##### Symbols

C	first integral of Euler-Lagrange equations, kg/sec
e	eccentricity, N.D.
E	energy per unit mass, $m^2/sec^2$
$\hat{f}$	unit thrust direction, N.D.
F	functional defined by equation (3) kg/sec
g	intermediate boundary equation
$\bar{G}$	gravity acceleration, $m/sec^2$
$\bar{G}_1, \bar{G}_2$	components of oblate gravity acceleration, $m/sec^2$
$G_m^*$	spherical earth gravity constant, $m^3/sec^2$
h	angular momentum per unit mass, $m^2/sec$
J	functional to be minimized, kg
m	mass, kg
N	total number of stages, N.D.
p	semi-latus rectum, m
r	radius, m
$r_p$	perigee radius, m
S	variational switching function, N.D.
t	time, sec
T	thrust, N
v	velocity, $m/sec$
x	state variable

$\hat{z}$	unit vector pointing at north pole, N.D.
$\beta$	mass flow rate, kg/sec
$\epsilon$	jump factor
$\eta$	Lagrange multiplier, kg/sec
$\lambda$	Lagrange multiplier, kg-sec/m
$\mu$	Lagrange multiplier, kg/m
$\sigma$	Lagrange multiplier, N.D.
$\psi$	pitch attitude, deg.
$\phi$	yaw attitude, deg.

##### Superscripts

.	time derivative
-	vector
$\wedge$	unit vector
f	final
o	initial

##### Subscripts

i, j, k, l, m, n	stage numbers
f	final
o	initial
d	desired
pk	parking orbit

##### Operators

.	dot product
x	cross product
d( )	differential
$\bar{\nabla}_x ( )$	gradient with respect to $\bar{x}$
$\frac{\partial ( )}{\partial ( )}$	partial derivative

#### Appendix B

##### Derivation of Optimum Control

As mentioned in the Analysis Section, the optimization of a trajectory to a circular synchronous equatorial orbit may be considered as the problem of optimizing a multi-stage launch vehicle to a particular final orbit. The optimization problem to be considered here begins at booster jettison, which is assumed to be a fixed position and velocity. The sustainer portion of the Atlas continues until propellant depletion. The sustainer is jettisoned and a few seconds later the first Centaur burn begins. Its duration is variable and must be optimized. The perigee radius of the parking orbit is fixed. The duration of the parking orbit may or may not be optimized. The parking orbit is not a true coast since a small acceleration is

maintained for propellant retention. The duration of the second Centaur burn must be optimized, followed by an optimum transfer orbit coast (a true coast), and a final burn of fixed total impulse. The analysis presented in this appendix to solve this problem is a special case of the analysis derived in Ref. 3, with an additional constraint - parking orbit perigee radius.

The variational problem to be solved is to find the steering program and various stage durations which maximize the payload capability of a multi-stage launch vehicle to a specified final orbit. The trajectory must satisfy certain initial, final, and intermediate conditions on the state variables. The thrust, propellant flow rate, and jettison weight for each stage are assumed to be constant. The equations of motion and constraints for each stage may be written as

$$\dot{\bar{v}} - \bar{G}(\bar{r}) - \frac{T_1}{m} \hat{f} = \bar{0} \quad (1a)$$

$$\dot{\bar{r}} - \bar{v} = \bar{0} \quad (1b)$$

$$\dot{m} + \beta_1 = 0 \quad (1c)$$

$$\hat{f} \cdot \hat{f} - 1 = 0 \quad (1d)$$

where  $\hat{f}$  is the unit thrust direction and  $\bar{G}(\bar{r})$  is the oblate earth gravity acceleration<sup>(6)</sup>, which may also be written

$$\bar{G}(\bar{r}) = G_1(r, \bar{r} \cdot \hat{z}) \hat{r} + G_2(r, \bar{r} \cdot \hat{z}) \hat{z} \quad (2)$$

(All symbols are defined in appendix A.) Suppose that each stage of the vehicle is numbered consecutively starting with the booster. For analysis purposes a stage change occurs when the thrust and/or propellant flow rate changes and/or a mass is jettisoned. A Bolza formulation of the variational problem is used<sup>(7)</sup>, and the functional to be minimized is written as in Ref. 3 as

$$J = -m_f + \sum_{i=2}^N \int_{t_{i-1}}^{t_i} F_i dt \quad (3)$$

where the functional  $F_i$  for each stage is

$$F_i = \bar{\lambda} \cdot \left[ \dot{\bar{v}} - \bar{G} - \frac{T_1}{m} \hat{f} \right] + \bar{\mu} \cdot \left[ \dot{\bar{r}} - \bar{v} \right] + \sigma(\dot{m} + \beta_1) + \eta(\hat{f} \cdot \hat{f} - 1) \quad (4)$$

The resulting Euler-Lagrange equations are

$$\dot{\bar{\lambda}} + \bar{\mu} = \bar{0} \quad (5a)$$

$$\dot{\bar{\mu}} + G_1 \frac{\bar{\lambda}}{r} + (\bar{\lambda} \cdot \hat{r}) \bar{\nabla}_r G_1 - G_1 (\bar{\lambda} \cdot \hat{r}) \frac{\hat{r}}{r} + (\bar{\lambda} \cdot \hat{z}) \bar{\nabla}_r G_2 = \bar{0} \quad (5b)$$

$$\dot{\sigma} - \frac{T_1}{m^2} \bar{\lambda} \cdot \hat{f} = 0 \quad (5c)$$

$$2\eta \hat{f} - \frac{T_1}{m} \bar{\lambda} = \bar{0} \quad (5d)$$

The optimum thrust direction  $\hat{f}$  is obtained by combining equations (1d) and (5d) and using the Weierstrass E-test. This procedure results in

$$\hat{f} = \hat{\lambda} \quad (6)$$

### Integrals of the Motion

Since  $F$  does not explicitly depend on time, an integral of the motion is

$$C + \bar{\lambda} \cdot \bar{G} + \bar{\mu} \cdot \bar{v} + \frac{T_1}{m} \lambda - \sigma \beta_1 = 0 \quad (7)$$

When a spherical gravity model is assumed (i.e.,  $\bar{G}(\bar{r}) = G_m^*/r^3 \bar{r}$ ), three additional integrals of the motion exist which are given by

$$\bar{\lambda} \times \bar{v} + \bar{\mu} \times \bar{r} = \text{constant}$$

Since  $\bar{\lambda}$ ,  $\bar{\mu}$ ,  $\bar{r}$ , and  $\bar{v}$  are all continuous except where an intermediate boundary condition is imposed (as will be shown later), the three integrals are constant across staging points where continuity holds. However, for the oblate gravity model used in this analysis, only a single component of the above vector integral is constant, as can be verified by differentiation with respect to time.

$$(\bar{\lambda} \times \bar{v} + \bar{\mu} \times \bar{r}) \cdot \hat{z} = \text{constant} \quad (8)$$

### Transversality Equation

The transversality equation for this problem is

$$dJ = \sum_{i=2}^N (C dt + \bar{\lambda} \cdot d\bar{v} + \bar{\mu} \cdot d\bar{r} + \sigma dm)_{t_{i-1}}^{t_i} - dm_f \quad (9)$$

which is set equal to zero for an optimal solution. Reference 3 shows that: 1)  $\bar{\lambda}$  and  $\bar{\mu}$  are continuous everywhere if there are no intermediate boundary conditions. If the intermediate boundary condition (assumed to occur at a staging point) is expressed as

$$g(\bar{r}, \bar{v}) = 0 \quad (10)$$

reference 8 shows that the discontinuities in  $\bar{\lambda}$  and  $\bar{\mu}$  are  $\epsilon \bar{\nabla}_{\bar{r}} g$  and  $\epsilon \bar{\nabla}_{\bar{v}} g$ , respectively. The variable  $\epsilon$  is used as an initial condition in the two point boundary value problem to satisfy the intermediate boundary condition (eq. (10)). 2) The equations that must be satisfied to optimize the duration of the powered and coast stages are derived in Ref. 3. The applicable results are presented here. Let  $j$  be the first optimized powered stage. Then for constant jettison weight the equation for optimizing stage  $l$  is

$$\sum_{i=j}^{l-1} (S_i^f - S_{i+1}^o) = 0 \quad (11)$$

where  $o$  and  $f$  refer to initial and final values and the  $S$  functions are defined as

$$S_i = \frac{C}{\beta_1} - \sigma = - \frac{\left[ \bar{\lambda} \cdot \bar{G} + \bar{\mu} \cdot \bar{v} + \frac{T_1}{m} \lambda \right]}{\beta_1}, \quad \beta_1 \neq 0 \quad (12a)$$

$$S_1 = 0, \beta_1 = 0 \quad (12b)$$

where the right side of equation (12a) is obtained by using equation (7). For coasting stages ( $\beta_1 = T_1 = 0$ ) to be optimized, the equation

$$C_1 = (\bar{\lambda} \cdot \bar{g} + \bar{\mu} \cdot \bar{v}) = 0 \quad (13)$$

must be satisfied for maximum payload.

3) For free initial or final state variable  $x$ , the required or final condition for maximum payload (Ref. 4) is

$$\bar{\lambda} \cdot \frac{\partial \bar{v}}{\partial x} + \bar{\mu} \cdot \frac{\partial \bar{r}}{\partial x} = 0 \quad (14)$$

#### Initial Conditions

If the initial position and velocity are specified, the initial values of any five of the six  $\bar{\lambda}$  and  $\bar{\mu}$  may be used as variable initial conditions in order to satisfy the required final conditions of the two point boundary value problem. In order to eliminate the difficulty associated with guessing at values of the multipliers, the values of  $\bar{\lambda}$  and  $\bar{\mu}$  can be expressed in terms of pitch and yaw attitude ( $\psi$  and  $\phi$ ) and rates ( $\dot{\psi}$  and  $\dot{\phi}$ ). These equations may be found in Ref. 4, appendix C. The values of  $\bar{\lambda}$  and  $\bar{\mu}$  are then calculated from:

$$\bar{\lambda} = \lambda \hat{\lambda} \quad (15a)$$

$$\bar{\mu} = -\lambda \hat{\lambda} - \dot{\lambda} \hat{\lambda} \quad (15b)$$

The value of  $\lambda$  can be set equal to unity without loss of generality. The initial value of  $\dot{\lambda}$  can be calculated in closed form, as will be shown by the following development.

#### Final Conditions

Final conditions for both the conventional and unconventional synchronous equatorial orbit mission require a circular orbit at synchronous orbit altitude with prescribed inclination. If the required inclination is non-zero, both the longitude of the ascending node and the injection point in the final orbit are free for optimization. As shown in Ref. 4, the corresponding auxiliary variational final conditions are

$$(\bar{\lambda} \times \bar{v} + \bar{\mu} \times \bar{r}) \cdot \hat{z} = 0 \quad (16a)$$

and

$$(\bar{\lambda} \times \bar{v} + \bar{\mu} \times \bar{r}) \cdot (\bar{r} \times \bar{v}) = 0 \quad (16b)$$

If the desired inclination is zero, equations (16a) and (16b) degenerate into one equation (zero inclination is equivalent to two final conditions,  $\bar{r} \cdot \hat{z} = 0$  and  $\bar{v} \cdot \hat{z} = 0$ ), and only equation (16a) must be satisfied.

Since equation (16a) is a constant of the motion (eq. 8), it may be satisfied at the beginning of the trajectory, and used to calculate  $\dot{\lambda}$ . However, it must first be verified that jump discontinuities in  $\bar{\lambda}$  and  $\bar{\mu}$  at intermediate boundary points do not change the value of the constant. This requires that

$$(\bar{\nabla}_v g \times \bar{v} + \bar{\nabla}_r g \times \bar{r}) \cdot \hat{z} = 0 \quad (17)$$

It will be shown later that equation (17) is satisfied for all functions  $g$  used herein.

The calculation of  $\dot{\lambda}$  proceeds as follows:

$$\begin{aligned} (\bar{\lambda} \times \bar{v} + \bar{\mu} \times \bar{r}) \cdot \hat{z} &= (\lambda \hat{\lambda} \times \bar{v}) \cdot \hat{z} \\ &\quad - (\lambda \hat{\lambda} \times \bar{r}) \cdot \hat{z} - (\dot{\lambda} \hat{\lambda} \times \bar{r}) \cdot \hat{z} = 0 \\ \dot{\lambda} &= \frac{\lambda(\hat{\lambda} \times \bar{v} - \hat{\lambda} \times \bar{r}) \cdot \hat{z}}{(\hat{\lambda} \times \bar{r}) \cdot \hat{z}} \end{aligned} \quad (18)$$

Computing  $\dot{\lambda}$  with equation (18) guarantees that equation (16a) will be satisfied.

#### Intermediate Conditions

As explained earlier, it is necessary to constrain the perigee radius at injection into the first parking orbit. Otherwise, the optimum solution would result in the parking orbit injection and/or the equator crossing occurring at very low altitudes, thus violating spacecraft heating constraints. Therefore, the intermediate constraint is

$$g(\bar{r}, \bar{v}) = r_p - r_{p,d} = 0 \quad (19)$$

where the desired value corresponds to the perigee altitude. By using equations found in Ref. 9, equation (19) can be written as

$$\frac{p}{1+e} - r_{p,d} = 0 \quad (20)$$

where

$$p = \frac{\bar{h} \cdot \bar{h}}{G_m^*} \quad (\text{semi-latus rectum}) \quad (21a)$$

$$e = \sqrt{1 + \frac{2E p}{G_m^*}} \quad (\text{eccentricity}) \quad (21b)$$

$$E = \frac{\bar{v} \cdot \bar{v}}{2} - \frac{G_m^*}{r} \quad (\text{energy per unit mass}) \quad (21c)$$

$$\bar{h} = \bar{r} \times \bar{v} \quad (\text{angular momentum per unit mass}) \quad (21d)$$

The required gradients are calculated to be

$$\bar{\nabla}_v g = \frac{h(\hat{h} \times \bar{r} - r_p^2 \bar{v})}{e G_m^*} \quad (22a)$$

$$\bar{\nabla}_r g = \frac{\frac{h}{G_m^*} (\bar{v} \times \hat{h}) - \hat{r} \frac{r_p^2}{r^2}}{e} \quad (22b)$$

It is easily shown that equation (17) is satisfied for the gradients in equation (22a) and (22b).

In fact, equation (17) is satisfied for any function  $g$  of  $r$ ,  $v$ ,  $h$  and  $\bar{r} \cdot \bar{v}$ . For such a function  $g$ ,

$$\bar{\nabla}_v g = \frac{\partial g}{\partial v} \hat{v} + \frac{\partial g}{\partial h} (\hat{h} \times \bar{r}) + \frac{\partial g}{\partial (\bar{r} \cdot \bar{v})} \bar{r}$$



$$\bar{\nabla}_{\bar{r}} g = \frac{\partial g}{\partial r} \hat{r} + \frac{\partial g}{\partial h} (\bar{v} \times \hat{h}) + \frac{\partial g}{\partial (\bar{r} \cdot \bar{v})} \bar{v} \quad (23)$$

and

$$\begin{aligned} \bar{\nabla}_{\bar{v}} g \times \bar{v} + \bar{\nabla}_{\bar{r}} g \times \bar{r} &= \frac{\partial g}{\partial v} \bar{v} \times \bar{v} \\ &+ \frac{\partial g}{\partial h} (\hat{h} \times \bar{r}) \times \bar{v} + \frac{\partial g}{\partial (\bar{r} \cdot \bar{v})} \bar{r} \times \bar{v} \\ &+ \frac{\partial g}{\partial r} \bar{r} \times \bar{r} + \frac{\partial g}{\partial h} (\bar{v} \times \hat{h}) \times \bar{r} \\ &+ \frac{\partial g}{\partial (\bar{r} \cdot \bar{v})} \bar{v} \times \bar{r} = \bar{0} \end{aligned} \quad (24)$$

Hence the value of  $\bar{\lambda} \times \bar{v} + \bar{\mu} \times \bar{r}$  is unaffected by the jump in  $\lambda$  and  $\mu$  resulting from a function  $g$  as defined above.

#### Boundary Value Problem

For the ATS-E mission, both fixed and optimum parking orbit coast times were considered. The transfer orbit coast time was always optimized, however, along with the durations of the first and second Centaur burns. Based on the preceding discussion of the transversality equation, the initial and final conditions for the two point boundary value problem are as follows for the case where the parking orbit coast time was optimized:

Initial Conditions	Final Conditions
$\psi$	$E_d$
$\dot{\psi}$	$r_d$
$\phi$	$\dot{r}_d$
$\dot{\phi}$	$r_{p,d}$ (Parking orbit)
$\epsilon$	$(\bar{r} \cdot \hat{z}) = 0$
$t_j$ (First Centaur Burn)	$(\bar{v} \cdot \hat{z}) = 0$
$t_k$ (Parking Orbit Coast)	$\sum_{i=j}^{k-1} (S_i^f - S_{i+1}^o) = 0$
$t_\ell$ (Second Centaur Burn)	$\sum_{i=j}^{\ell-1} (S_i^f - S_{i+1}^o) = 0$
$t_m$ (Transfer Orbit Coast)	$(\bar{\lambda} \cdot \bar{G} + \bar{\mu} \cdot \bar{v}) = 0$

(25)

If the desired final inclination is non-zero, then  $(\bar{r} \cdot \hat{z})$  and  $(\bar{v} \cdot \hat{z}) = 0$  are replaced by  $i_d$  and  $(\bar{\mu} \times \bar{r} + \bar{\lambda} \times \bar{v}) \cdot (\bar{r} \times \bar{v}) = 0$ . If the parking orbit coast time is fixed, then an initial and final condition are removed. These are  $t_k$  and

$$\sum_{i=j}^{k-1} (S_i^f - S_{i+1}^o) = 0$$

It should be recognized that there may be any number of fixed stages between  $t_j$  and  $t_k$ , etc. Also, the last three final conditions are evaluated at intermediate points in the trajectory.

#### Appendix C

##### Two Point Boundary Value Problem

The following technique was devised to systematically proceed from a simple, easily converged problem to the solution of the two point boundary value problem for a circular synchronous equatorial orbit.

A trajectory is obtained to a slightly elliptical (parking) orbit with the desired perigee radius without plane change with a 90° launch azimuth. This problem converges easily. Then the ascent burn time is fixed at the value obtained and a variable length parking orbit coast, a fixed parking orbit perigee radius and a second burn are added. This problem is targeted to the desired apogee and 180° argument of perigee for first equator crossing second burn. An inclination decrease of about two degrees is then added to these final conditions and the problem is retargeted to the augmented final conditions. Now the transfer orbit coast (variable) and apogee burn (fixed or variable) are added. This trajectory is integrated to the end with the converged initial guesses from the last step. The final conditions achieved will frequently be far from a circular synchronous equatorial orbit. However, specify the final conditions actually achieved as the desired ones, and optimize the problem. The parking orbit coast, second burn, and transfer orbit coast durations will change. Now alter the achieved final conditions toward the desired ones judiciously in steps, retargeting at each step. In this manner, the desired final orbit conditions may be obtained. Now the ascent burn duration may be optimized. Any sizable change in a constraint or final condition is best achieved by proceeding in steps. The problem is quite nonlinear. Attempts to plot initial conditions as functions of the final conditions for extrapolation purposes were made. They were generally unsuccessful.

#### References

1. Hoelker, R. F. and Silber, R., "Injection Schemes for Obtaining a Twenty-Four Hour Orbit," Aerospace Engineering, Vol. 20, No. 1, Jan. 1961, pp. 28-29, 76-84.
2. Rider, L., "Characteristic Velocity Requirements for Impulsive Thrust Transfers Between Non Co-Planar Circular Orbits," American Rocket Society Journal, Vol. 31, No. 3, Mar. 1961, pp. 345-351.
3. Teren, F. and Spurlock, O. F., "Payload Optimization of Multistage Launch Vehicles," TN D-3191, 1966, NASA, Cleveland, Ohio.
4. Teren, F. and Spurlock, O. F., "Optimal Three Dimensional Launch Vehicle Trajectories with Attitude and Attitude Rate Constraints," TN D-5117, 1969, NASA, Cleveland, Ohio.

5. Spurlock, O. F. and Teren, F., "A Trajectory Code for Maximizing the Payload of Multistage Launch Vehicles," TN D-4729, 1968, NASA, Cleveland, Ohio.
6. Clarke, V. C., Jr., "Constants and Related Data Used in Trajectory Calculations at the Jet Propulsion Laboratory," JPL-TR-32-273, May 1962, Jet Propulsion Lab., California Inst. Tech., Pasadena, Calif.
7. Bliss, G. A., Lectures on the Calculus of Variations, University of Chicago Press, 1946.
8. Pontryagin, L. S., et al., The Mathematical Theory of Optimal Processes, Interscience, New York, 1962.
9. Dobson, W. F., Huff, V. N., and Zimmerman, A. V., "Elements and Parameters of the Osculating Orbit and Their Derivatives," TN D-1106, 1962, NASA-Cleveland, Ohio.

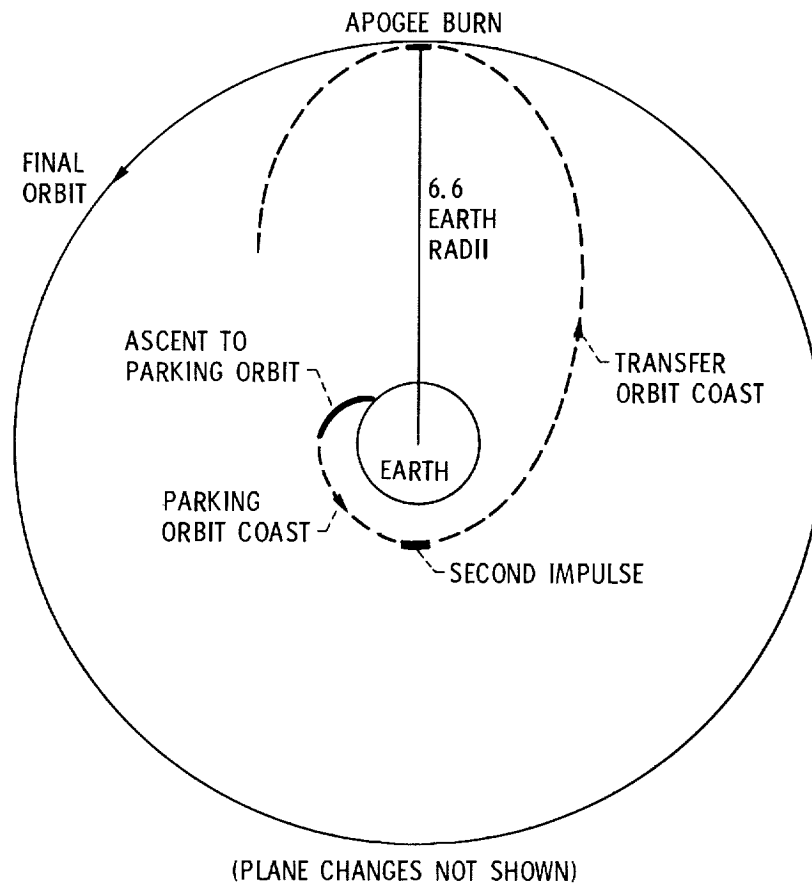


Figure 1. - Conventional trajectory to circular synchronous equatorial orbit.

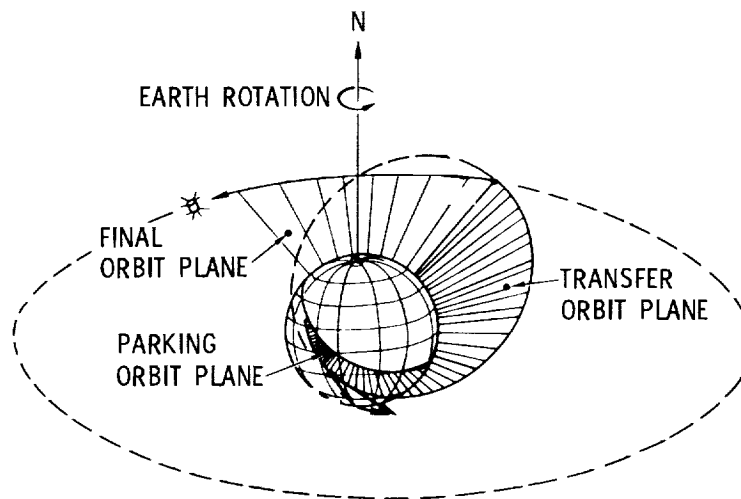


Figure 2. - Circular synchronous equatorial orbit ascent profile.

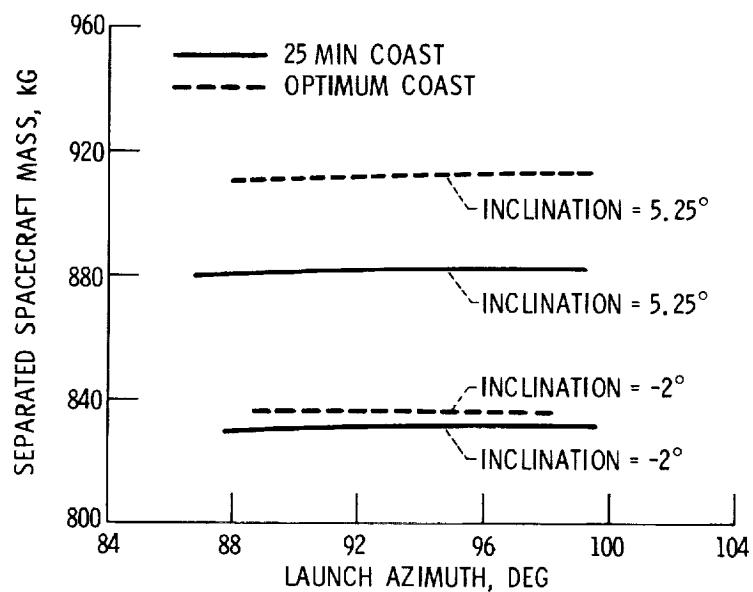


Figure 3. - Separated spacecraft mass as a function of launch azimuth.

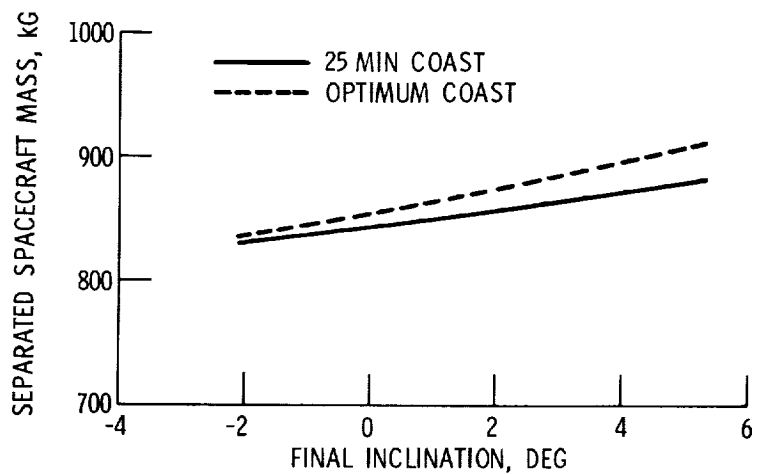


Figure 4. - Separated spacecraft mass as a function of final inclination.

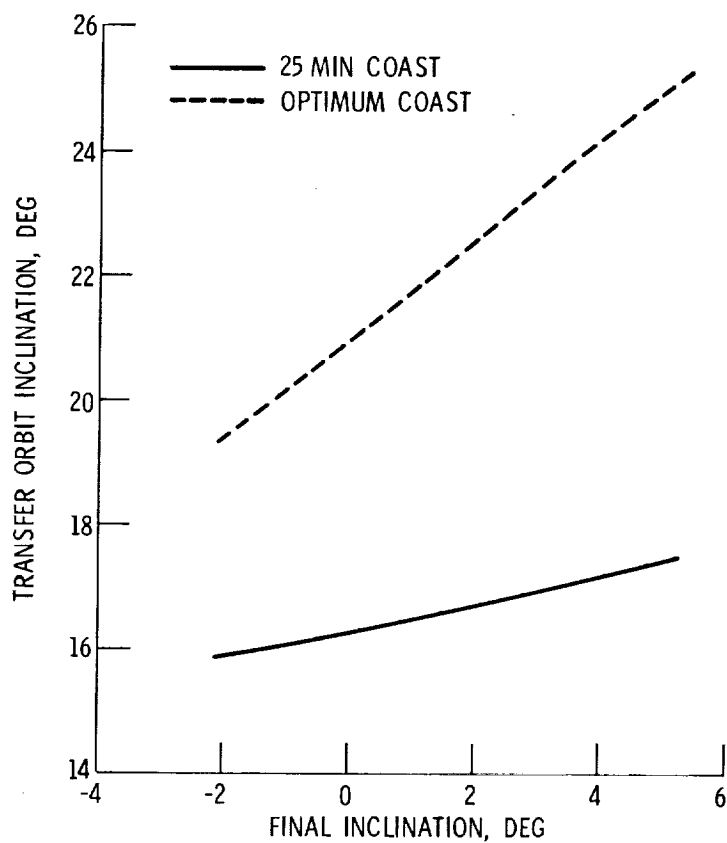


Figure 5. - Transfer orbit inclination as a function of final inclination.

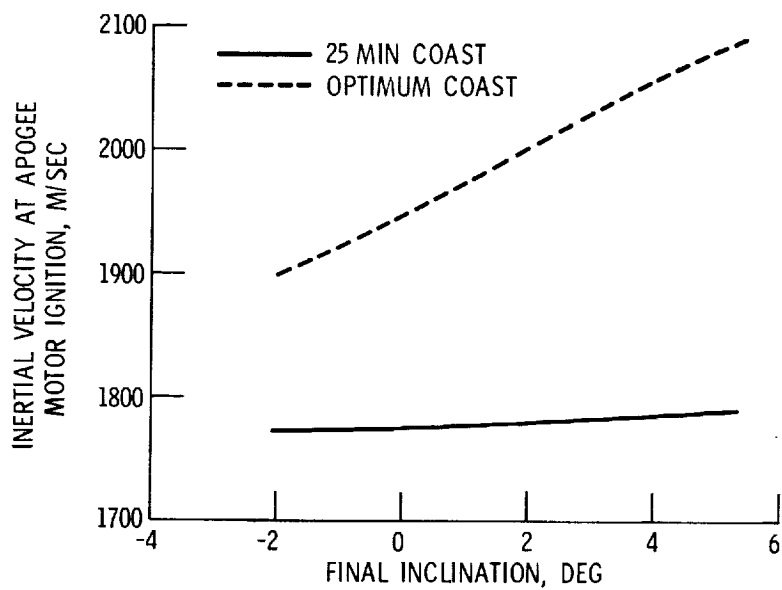


Figure 6. - Inertial velocity at apogee motor ignition as a function of final inclination.

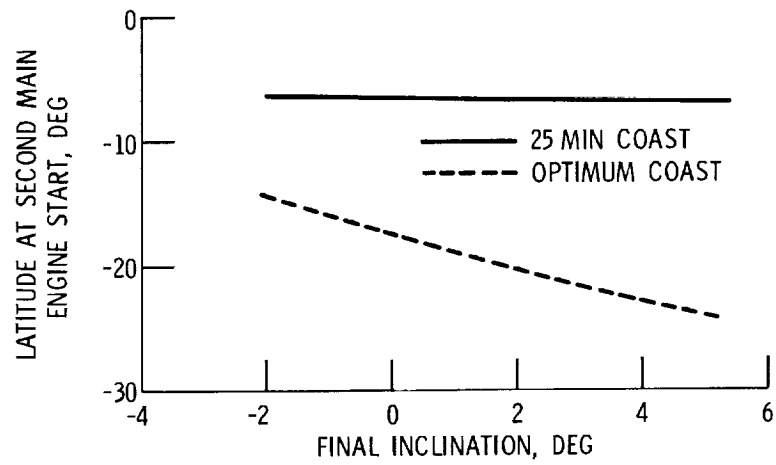


Figure 7. - Latitude at second main engine start as a function of final inclination.

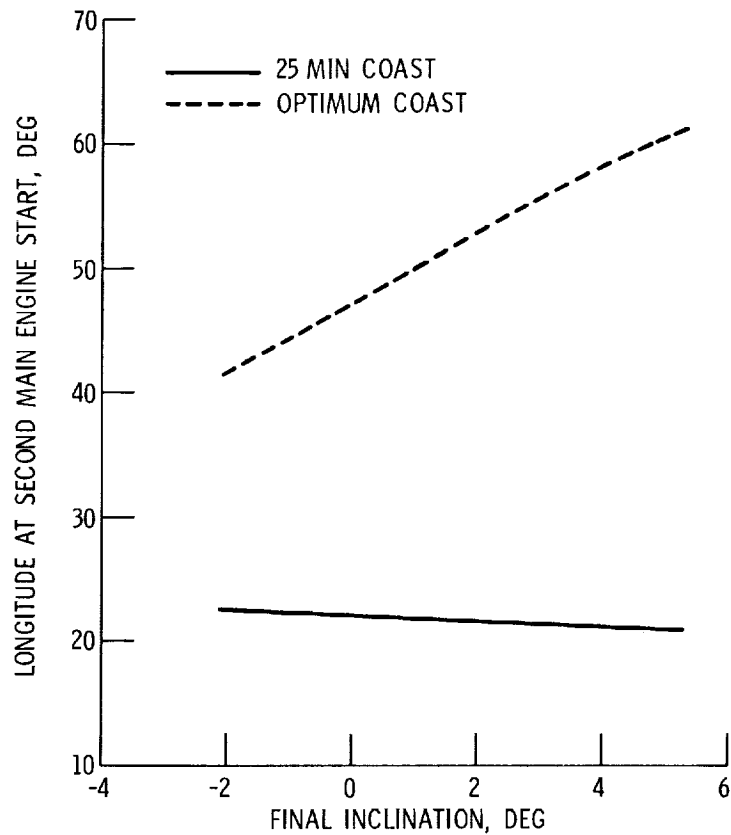


Figure 8. - Longitude at second main engine start as a function of final inclination.

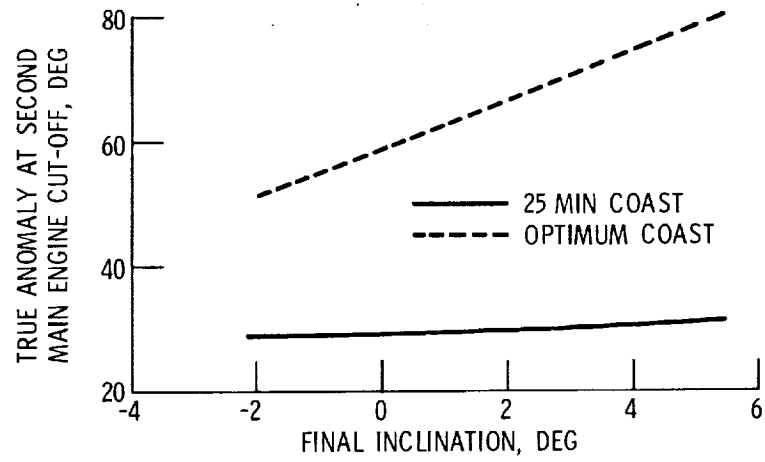


Figure 9. - True anomaly at second main engine cut-off as a function of final inclination.

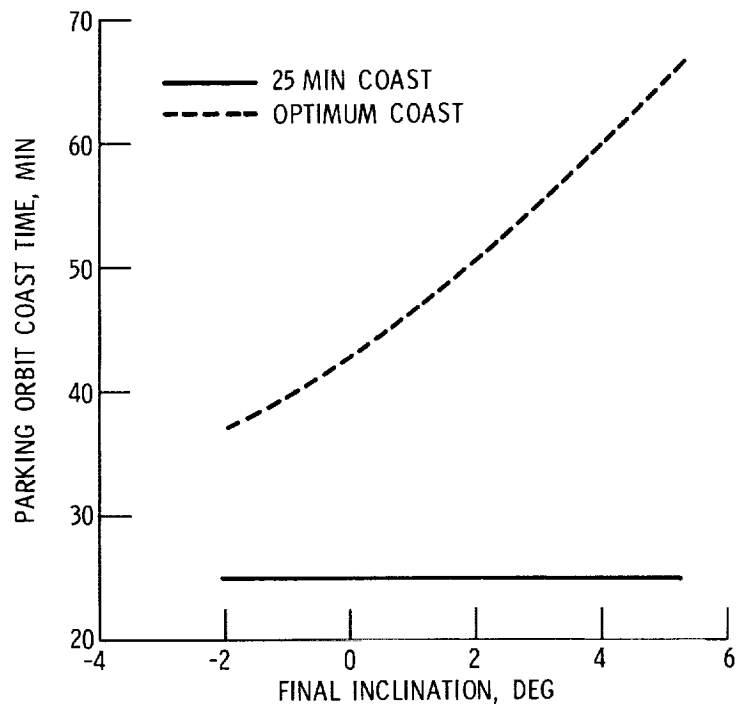


Figure 10. - Parking orbit coast time as a function of final inclination.

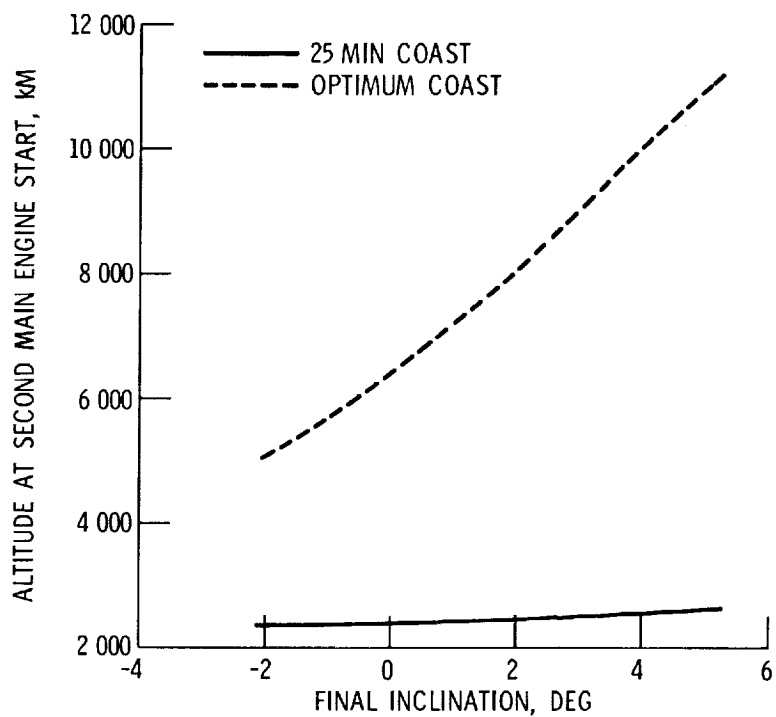


Figure 11. - Altitude at second main engine start as a function of final inclination.

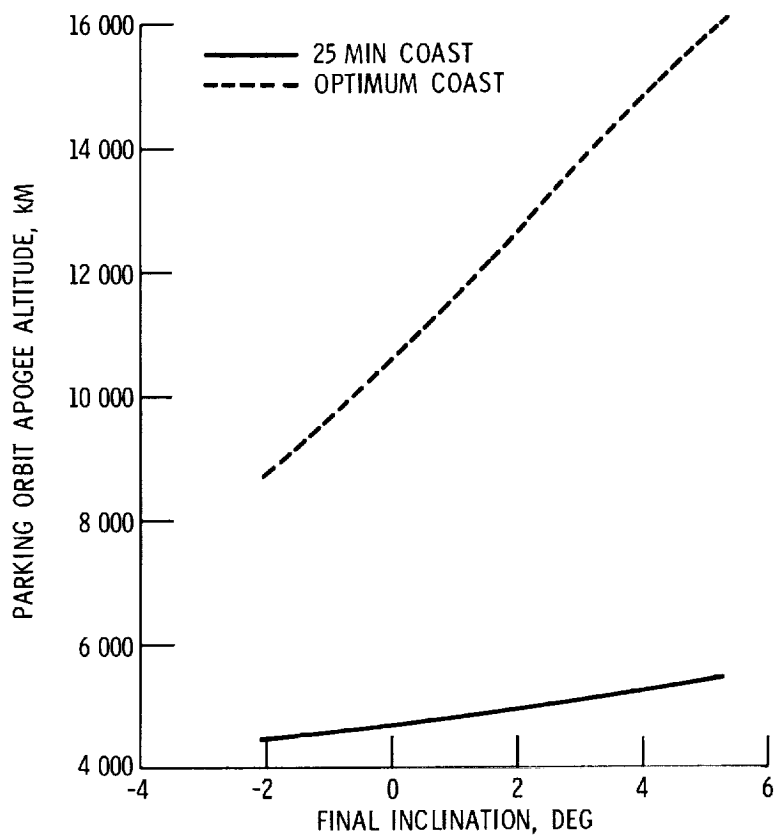


Figure 12. - Parking orbit apogee altitude as a function of final inclination.



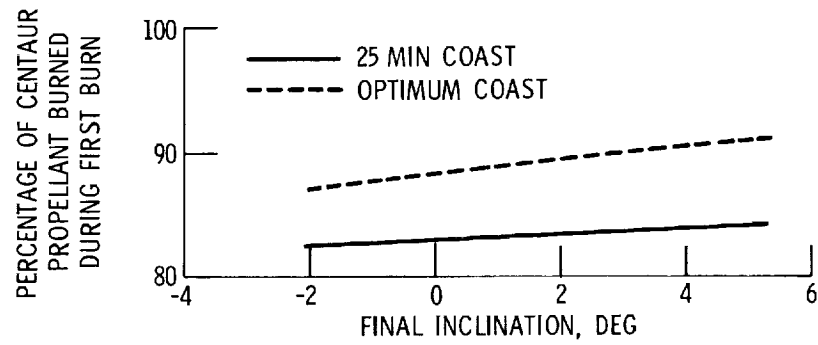


Figure 13. - Percentage of Centaur propellant burned during first burn as a function of final inclination.

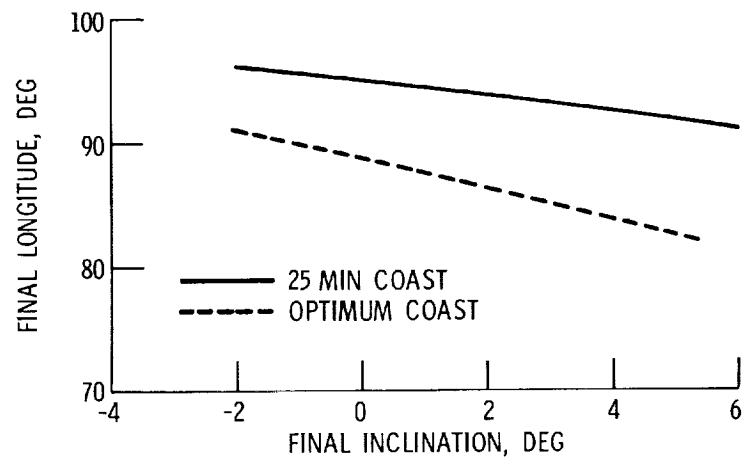


Figure 14. - Final longitude as a function of final inclination.